Physics and Chemistry of Minerals (2019) 46:771–781
https://doi.org/10.1007/s00269-019-01038-w

ORIGINAL PAPER

Crystal structure of norsethite-type $BaMn(CO_3)_2$ and its pressure-induced transition investigated by Raman spectroscopy

Wen Liang[1] · Lin Li[2,6] · Yuan Yin[1,4] · Rui Li[1,4] · Zeming Li[1,4] · Xiqiang Liu[1,4] · Chaoshuai Zhao[1,4] · Shuguang Yang[3,4] · Yong Meng[3] · Zengsheng Li[5] · Yu He[1] · Heping Li[1]

Received: 10 January 2019 / Accepted: 21 May 2019 / Published online: 30 May 2019

Abstract

Single crystals of norsethite-type carbonate $BaMn(CO_3)_2$ up to 200 μm in size were synthesized in a closed cavity under high pressure–temperature (P–T) conditions. Electron microprobe analyses revealed the composition of 49.00–49.09 wt% BaO and 22.66–22.74 wt% MnO, which correspond well to the ideal formula of $Ba_{1.0}Mn_{1.0}(CO_3)_2$. Accurate crystalline structural data were determined from single crystal X-ray diffraction (XRD). The $R\bar{3}c$ space-group with a doubled c-axis and $R\bar{3}m$ space-group were used to refine the crystal structure of $BaMn(CO_3)_2$. It is proved that $R\bar{3}m$ is the most probable space-group for the $BaMn(CO_3)_2$ crystal structure because no superstructure reflections were observed in the X-ray images. The unit cell parameters were identified to be $a = 5.0827(2)$ Å and $c = 17.2797(10)$ Å in the rhombohedral symmetry of the $R\bar{3}m$ space-group with a final R-value of 0.0184. High-pressure Raman spectroscopy was performed up to 10 GPa at room temperature, and Raman band shifts ($\frac{dv_i}{dP}$) were quantified. Each Raman vibration underwent resolvable splitting and the corresponding $\frac{dv_i}{dP}$ showed a pronounced jump as the pressure reached 3.8 GPa arising from a pressure-induced transition.

Keywords Norsethite-type $BaMn(CO_3)_2$ · Single crystal growth · Single crystal X-ray diffraction · High-pressure Raman spectroscopy

Introduction

Double carbonates $AB(CO_3)_2$ with typical layer-structures have widespread geological distribution in surface sediments and oceanic crusts. These are commonly found as dolomite $CaMg(CO_3)_2$, ankerite $CaFe(CO_3)_2$, and kutnohorite $CaMn(CO_3)_2$ (Reeder and Dollase 1989; Peacor et al. 1987; Ross and Reeder 1992). Compared to calcite-type carbonates, many double carbonates form heterotype structures with two distinct cation sites (A- and B-sites) interconnected with CO_3^{2-} ions; in some cases, R-centered trigonal symmetry is maintained. The essential layer-structure formation originates from the limited miscibility of the solid solutions, which is caused by the significant difference between the A and B ionic radii (Reeder 1983). As a typical double carbonate, norsethite $BaMg(CO_3)_2$ is a rare mineral existing sparsely in different geological settings. Firstly, it has been found in the sedimentary Green River Formation in Wyoming, USA (Mrose et al. 1961), and later, at other locations worldwide (Sundius and Blix 1965; Kapustin 1965; Steyn and Watson 1967; Platt and Woolley 1990; Damyanov et al. 1996; Secco and Lavina 1999; Onac 2002; Zidarov et al.

Electronic supplementary material The online version of this article (https://doi.org/10.1007/s00269-019-01038-w) contains supplementary material, which is available to authorized users.

✉ Wen Liang
liangwen@mail.gyig.ac.cn

✉ Heping Li
liheping@vip.gyig.ac.cn

1 Key Laboratory of High Temperature and High Pressure Study of the Earth's Interior, Institute of Geochemistry, Chinese Academy of Sciences, Guiyang 550081, China

2 State Key Laboratory of Geological Processes and Mineral Resources, China University of Geosciences, 29 Xueyuan Road, Beijing 100083, China

3 State Key Laboratory of Ore Deposit Geochemistry, Institute of Geochemistry, Chinese Academy of Sciences, Guiyang 550081, China

4 University of Chinese Academy of Sciences, Beijing 100049, China

5 Shandong Geological Sciences Institute, Jinan 250013, China

6 Institute of Science Research, China University of Geosciences, 29 Xueyuan Road, Beijing 100083, China

2009). Composition analysis of these natural norsethite carbonates revealed that Mg^{2+} cations were often substituted by a small amount of Mn^{2+} ions forming Mn-bearing norsethite. To date, the highest reported Mn content in natural norsethite was 20 mol% by Zidarov et al. (2009).

Recently, the physical/chemical properties and formation mechanisms of norsethite have been the subject of great concern to deepen understanding of its role in the coupled geochemical cycles of carbon and barium. Since the end-member phase is an important component for quantitative research into natural Mn-bearing norsethite, many experimental reports have focused on norsethite $BaMg(CO_3)_2$ and norsethite-type $BaMn(CO_3)_2$, emphasizing the kinetic processes of ordered growth on the carbonate surfaces, isotope fractionation and the pressure-induced transition that may occur during subduction (Hood et al. 1974; Lepland and Stevens 1998; Lepland et al. 2000; Böttcher 2000; Böttcher et al. 2012; Zheng and Böttcher 2014; Pippinger et al. 2014; Lindner et al. 2017, 2018; Lindner and Jordan 2018).

Besides these interesting results, details about the crystalline structure and space-group symmetry of norsethite $BaMg(CO_3)_2$, and its synthetic analogue remained unclear for a long time. Even the atomic arrangement of this carbonate is topologically related to that of dolomite—the larger ratio between the radii of the Ba^{2+}/Mg^{2+} ions compared to that of Ca^{2+}/Mg^{2+} causes a distinct rotation of the carbonate group around [001]. Three structure models based on the space-group symmetries have been discussed extensively: *R32* (model 1); ordered $R\bar{3}m$ (model 2); and strongly displaced and statistically occupied O atom positions (model 3) (Lippmann 1968; Effenberger and Zemann 1985; Secco and Lavina 1999). From powder XRD analyses of synthetic $BaMg(CO_3)_2$, Lippmann (1968) considered model 1 as the most probable, but mentioned the possibility of verifying models 2 or 3. Later, Effenberger and Zemann (1985) used the same material for their single crystal X-ray analyses. However, they could not verify higher significance for any of the three models. Consequently, they described the crystal structure of $BaMg(CO_3)_2$ based on the highest symmetry under discussion (model 2) even though they could not exclude with certainty models 1 or 3. They mentioned the large anisotropic displacement of the O atoms parallel to (0001). Subsequently, Secco and Lavina (1999) also favoured model 2. Most recently, Effenberger et al. (2014) refined the crystalline structure of $BaMg(CO_3)_2$ using crystals synthesized by Lippmann (1968), but based on data collected with a four-circle diffractometer equipped with an X-ray microfocus-source and a pixel detector. The sensitivity of the new generation of X-ray detectors allowed the observation of superstructure reflections along the c^* direction. Consequently, $c' = 2c$. The crystalline structure refinement in space-group $R\bar{3}c$ resulted in an ordered atomic arrangement with moderate displacement parameters of all atoms.

As Mn is an essential constituent of the norsethite of certain localities, knowledge of $BaMn(CO_3)_2$ is important for constructing quantitative models of natural norsethite. Structural analogy or even isotype with $BaMg(CO_3)_2$ was proven by Raman spectroscopy and X-ray powder patterns (Böttcher et al. 2012; Schmidt et al. 2013). However, the crystalline structure of $BaMn(CO_3)_2$ is yet to be determined due to unavailability of single crystals.

Of particular interest is: (1) results of tentative isotype of the crystal structures of $BaM(CO_3)_2$ (M = Mg, Mn) hints at the possibility of a (continuous) solid solution between $BaMg(CO_3)_2$ and $BaMn(CO_3)_2$. Thus, the atomic arrangement of natural Mn-bearing norsethite, $Ba(Mg,Mn)(CO_3)_2$, might be consistent with the crystal structure model of $BaMg(CO_3)_2$ (Effenberger et al. 2014). Otherwise, it would be necessary to consider the influence of Mn^{2+} ions substituting for Mg^{2+} ions in the crystalline structure and space-group symmetry in Mn-bearing norsethite. (2) A tentative order of the carbonate groups along [001] based on $c' = 2c$ and space-group $R\bar{3}c$ as found for $BaMg(CO_3)_2$ so far has not been verified for $BaMn(CO_3)_2$. Schmidt et al. (2013) performed powder diffraction investigations using conventional X-ray tubes and detectors. Hypothetical superstructure reflections along c^* requires validation by high accuracy single crystal data (either synchrotron radiation and/or a highly sensitive detector. (3) Mn-rich norsethite or even a mineral close to the end-member composition $BaMn(CO_3)_2$, could exist in some specific geological environments (Zidarov et al. 2009; Böttcher et al. 2012). Thus, knowledge of the crystalline structure of $BaMn(CO_3)_2$ is essential for further discussion of the incorporation of Mn^{2+} ions into norsethite.

In this paper, high quality single crystals of norsethite-type $BaMn(CO_3)_2$ were synthesized under high P–T conditions. The crystalline structure and space-group symmetry were determined using single crystal XRD analyses. The high-pressure properties and pressure-induced transition were investigated by Raman spectroscopy.

Experimental methods

$BaMn(CO_3)_2$ powder samples were prepared under high P–T conditions following a simple solid reaction (Chang 1964; Schmidt et al. 2013), and single crystals were synthesized based on the high P–T annealing method reported by Liang et al. (2018). The entire synthesis process consisted of two parts: powder sample preparation and single crystal growth.

The first step in the experiment was the powder sample preparation. 10 g of $MnCO_3$ (99.99%, Alfa Aesar) and $BaCO_3$ (99.99%, Alfa Aesar) at a molar ratio 1:1 were weighed to ensure accurate stoichiometry. The powder was then mixed and ground with acetone in an agate mortar. A sample pellet 6 mm in diameter and 3 mm in length was

prepared and covered with 0.025 mm thick gold foil (99%, Alfa Aesar). The high P–T solid reaction was performed on a DS 6 × 600t cubic-anvil-type apparatus using h-BN as the pressure medium and a graphite heater at 3 GPa and 700 °C for 2 h. The pressure was reduced to ambient after quenching at ambient conditions, and the sample was obtained after removing the gold coverage. Powder XRD was used to verify the $BaMn(CO_3)_2$ single phase without any observed impurities.

The second step in the experiment involved analysis of the single crystal growth. The powder sample obtained from the first step and anhydrous $H_2C_2O_4$ were mixed in a molar ratio of 1:0.05 and formed into a pellet 6 mm in diameter and 3 mm in length. Then, the sample was sealed in a platinum 0.1 mm thick capsule with 40 µL of deionized water. The sample was re-treated under 3 GPa and 700 °C for 48 h before being quenched at ambient conditions. Finally, the platinum capsule was opened and the finished sample removed. The single crystals were examined under a plane polarized microscope, and the micro-composition was quantified using electron probe analysis.

A piece of single crystal 30 µm × 50 µm × 50 µm in size was used for single crystal XRD. Single crystal XRD measurements were obtained at ambient conditions with a Rigaku Xtalab PRO diffractometer system and HyPix-6000HE detector. The intensity data were collected using a 1.2 kW water-cooled microfocus-source with a rotating Mo anode and multilayer mirrors, and an equipped CCD detector with a frame size of 100 times/100 µm and 775 times/770 unit pixels. The monochromator is a series of 150 mm multilayer mirrors, with a divergence less than 4.8 m RAD. The work distance between the crystal and the detector was kept greater than 30 mm. An empirical absorption correction was applied based on the multi-scan technique using spherical harmonics, and implemented with the SCALE3 ABSPACK scaling algorithm. The range of data collection was $7° \le 2\theta \le 60°$ and the number of variable parameters (p) was 14. A weighting scheme is defined as $w = 1/[\sigma^2(F_o^2) + (0.1000P)^2]$ where $P = (F_o^2 + 2F_c^2)/3$. $R = \sum||F_0| - |F_c||/\sum|F_0|$. The electron density maximum was 0.889 and minimum −0.776. Data processing was performed with the CrysAlisPro processing program. The structures were determined using the direct methods of the SHELXS package and refined with the anisotropic approach using the SHELXL program (Sheldrick 2008).

For high pressure Raman spectroscopy experiments, a piece of the single crystal with a diameter of ~80 µm and a thickness of ~30 µm was selected as the initial sample. A rhenium gasket was indented to a thickness of 60 µm using a pair of diamond anvils with 400 µm flat culets. A 220 µm diameter hole was then drilled into the pre-indented gasket and used as a sample chamber. The initial sample was loaded into the sample chamber of a DAC together with several ruby spheres close to the sample for pressure calibration, and a 4:1 methanol–ethanol mixture was loaded into the sample chamber as the pressure medium.

Results and discussion

Powder sample preparation of norsethite-type $BaMn(CO_3)_2$ under high P–T conditions

Following norsethite $BaMg(CO_3)_2$ being found in nature (Mrose et al. 1961), Chang (1964) synthesized powder samples of the double carbonates $BaMg(CO_3)_2$ and $BaMn(CO_3)_2$ at 500 °C and 15 kbars for 25 h. Recently, Schmidt et al. (2013) prepared a $BaMn(CO_3)_2$ powder sample using two different methods at both low P–T and high P–T conditions, and found no significant difference between either sample. From these previous studies, the high P–T method was proven to be more effective at synthesizing $BaMn(CO_3)_2$. However, even though Schmidt et al. (2013) used almost the same P–T experimental conditions as those reported by Chang (1964), the as-synthesized sample was identified as consisting of the main phase of $BaMn(CO_3)_2$, but also contained some impurities of $BaCO_3$, $MnCO_3$, and a trace of Mn_3O_4. Thus, optimizing the high P–T experimental conditions for $BaMn(CO_3)_2$ synthesis requires further improvements and controlling crystal growth is believed to be the premise.

In this regard, we considered the higher P–T conditions of 3 GPa and 700 °C to accelerate the solid solution reaction, while the volume of the sample was reduced to ensure a smaller P–T gradient in the assembly. High P–T conditions decomposed the $MnCO_3$ reaction in the same assembly that was performed at 0.2 GPa and 700 °C for 1 h. The final product from the powder XRD was identified as a mixture of $MnCO_3$ and MnO, as seen in the supplementary Fig. 1. The observation of MnO could provide direct evidence that the oxygen fugacity conditions in our high P–T experiments were different from that of Schmidt et al. (2013), thereby ensuring the stability of Mn^{2+} in the $MnCO_3$ and $BaMn(CO_3)_2$.

During powder sample synthesis, the $MnCO_3$ and $BaCO_3$ mixture at a mole ratio of 1:1 easily and quickly formed a solid solution at 3 GPa and 700 °C within a short period of 2 h, and the grinded powder appeared light blue. The powder XRD patterns of the as-synthesized sample, given in Fig. 1, were consistent with previously published data (Chang 1964; Böttcher et al. 2012), in which all the diffraction peaks were indexed according to the $BaMn(CO_3)_2$ single crystal data obtained in this work. This result confirms the existence of $BaMn(CO_3)_2$ with a nearly ideal 1:1 cationic stoichiometry. It also indicates that $MnCO_3$ (calcite-type) and $BaCO_3$ (aragonite-type) could react through a high

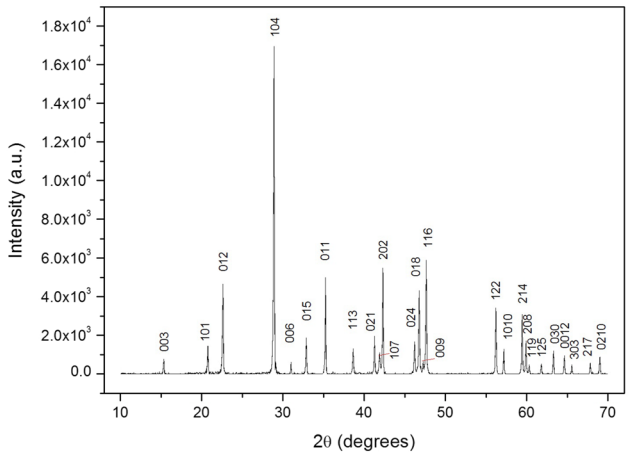

Fig. 1 The XRD patterns of synthetic $BaMn(CO_3)_2$ powder

P–T solid reaction forming $BaMn(CO_3)_2$ (norsethite-type). Based on this, we speculate the possible high P–T formation of norsethite-type carbonates. That is, if witherite $BaCO_3$ together with other calcite-type carbonates in sediments (e.g.: $CaCO_3$, $MgCO_3$, and $MnCO_3$) can be transferred into the deep mantle by subduction of the oceanic lithosphere and enriched in carbonates magma, norsethite-type carbonates could be formed under sufficient P–T conditions (3 GPa corresponds to ~ 90 km depth). Alternatively, in some particular cases, norsethite-type carbonates could survive in igneous carbonatite from the Earth's interior.

Single crystal growth of norsethite-type $BaMn(CO_3)_2$ under high P–T

Norsethite-type $BaMn(CO_3)_2$ crystals were cultivated in the presence of water in the cavity under high P–T conditions, which were based on the experience of the single crystal growth of siderite (Liang et al. 2018). However, the process here was more complex. The key to single crystal growth is to use the powder sample as a starting material to ensure that the initial Ba/Mn ratios in the saturated solution are in strict accordance with the initial 1:1 molar ratio. The reaction equilibrium can be described as:

$$\underset{\text{(powder)}}{BaMn(CO_3)_2} \overset{\text{dissolution reaction}}{\leftrightarrow} \underset{\text{(saturated solution)}}{Ba^{2+}_{(aq)} + Mn^{2+}_{(aq)} + 2CO^{2-}_{3\ (aq)}} \overset{\text{crystallization reaction}}{\leftrightarrow} \underset{\text{(crystals)}}{BaMn(CO_3)_2},$$

whereas a trace amount of CO_2 acts as the acidic medium for the solution to promote $BaMn(CO_3)_2$ powder dissolution.

Due to the fact that almost no impurities of $MnCO_3$ and $BaCO_3$ were found in the initial $BaMn(CO_3)_2$ powder or the final $BaMn(CO_3)_2$ crystals, we infer that both the dissolution reaction and the crystallization reaction reached an ideal equilibrium. Thus, based on the concentration of Ba^{2+} and Mn^{2+} with a molar ratio of 1:1, $BaMn(CO_3)_2$ could have a lower solubility product constant (K_{sp}) than that of $MnCO_3$ and $BaCO_3$ and thereby be preferentially precipitated and crystallized from the solution.

For comparison, we also performed the single crystal growth under the same experimental conditions using the $MnCO_3$ and $BaCO_3$ mixture with a molar ratio of 1:1. We found that $BaMn(CO_3)_2$ crystals were present in the final product in addition to a significant amount of $MnCO_3$ and $BaCO_3$ crystals. A potential explanation is given by the reactions (1)–(5) below:

$$BaCO_3 \overset{\text{dissolution reaction}}{\leftrightarrow} Ba^{2+}_{(aq)} + CO^{2-}_{3\ (aq)}\ K_{sp\_}BaCO_3 = \left[Ba^{2+}\right]\left[CO^{2-}_3\right], \quad (1)$$

$$MnCO_3 \leftrightarrow Mn^{2+}_{(aq)} + CO^{2-}_{3\ (aq)}\ K_{sp\_}MnCO_3 = \left[Mn^{2+}\right]\left[CO^{2-}_3\right], \quad (2)$$

$$xBaCO_3 + yMnCO_3 \leftrightarrow xBa^{2+}{}_{(aq)} + yMn^{2+}{}_{(aq)} + (x+y)CO^{2-}_{3\ (aq)} (x \neq y), \quad (3)$$

$$xBa^{2+}{}_{(aq)} + yMn^{2+}{}_{(aq)} + (x+y)CO^{2-}_{3\ (aq)} \overset{\text{crystallization reaction}}{\leftrightarrow} BaMn(CO_3)_2 \downarrow + MnCO_3 \downarrow x < y \text{ or,} \quad (4)$$

$$xBa^{2+}{}_{(aq)} + yMn^{2+}{}_{(aq)} + (x+y)CO^{2-}_{3\ (aq)} \leftrightarrow BaMn(CO_3)_2 \downarrow + BaCO_3 \downarrow x > y. \quad (5)$$

Despite the precondition that the solid phase of $MnCO_3$ and $BaCO_3$ be artificially set to the initial molar ratio 1:1, the initial Ba/Mn ratios in the saturated solution deviated from 1:1 ($x \neq y$) because of the differences in the K_{sp} between the $BaCO_3$ and $MnCO_3$, as shown in reactions (1)–(3). In this case, the precipitation and crystallization of $BaMn(CO_3)_2$, $MnCO_3$, and $BaCO_3$ occurred simultaneously, as shown in reactions (4) and (5). Considering the case when $x < y$, once the $MnCO_3$ precipitation nucleated at high P–T conditions (4), $MnCO_3$ crystals grew rapidly on the crystal nuclei to reduce the surface energy resulting in a decreased Mn^{2+} concentration. This caused the Ba/Mn ratios in the solution to change further (from $x < y$ to $x > y$) so that a similar crystallization reaction for the $BaCO_3$ in reaction (5) could occur. Since the grain boundary effect can prevent the formation of $BaMn(CO_3)_2$, the entire crystal growth process becomes relatively complex due to the competition between the crystallization reactions of $BaMn(CO_3)_2$, $MnCO_3$, and $BaCO_3$. In addition, some inclusions of relatively small

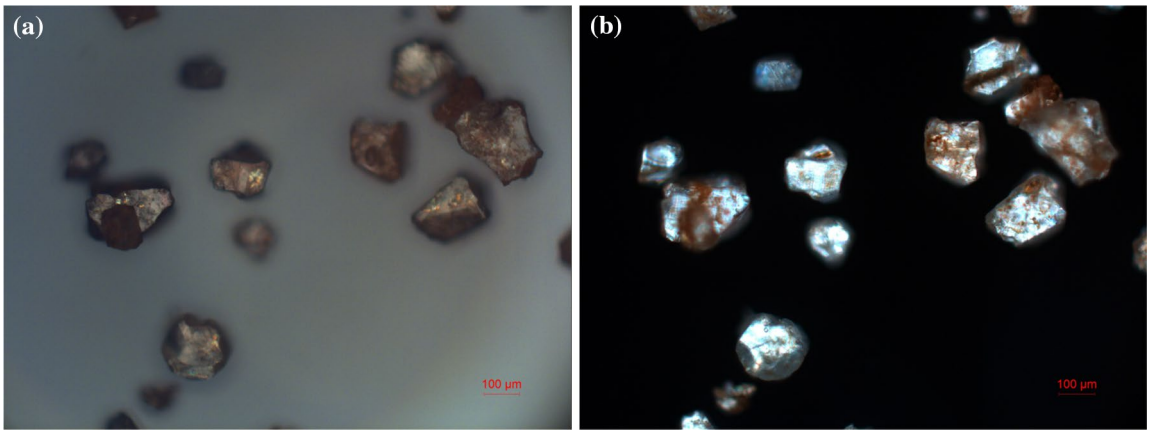

Fig. 2 The micrograph for $BaMn(CO_3)_2$ single crystals observed in a polarizing microscope with reflected light (**a**) and transmitted light (**b**)

$MnCO_3$ and $BaCO_3$ crystals appeared in the inner parts of the $BaMn(CO_3)_2$ crystals. The quality of the $BaMn(CO_3)_2$ single crystals was very poor and could not be used for single crystal XRD analyses. Consequently, the formation and crystal growth of $BaMn(CO_3)_2$ is closely dependent on the initial Ba/Mn ratios in the saturated solution, which is consistent with the results from Böttcher et al. (2012).

Morphology and composition of $BaMn(CO_3)_2$ crystals

Microscope observations revealed that the sizes of $BaMn(CO_3)_2$ single crystals reached up to 200 μm and exhibited a flaky morphology, as shown in Fig. 2. Under plane polarized light, the grown $BaMn(CO_3)_2$ crystals were transparent with a light blue luster, while the surface inclusions appeared yellowish-brown. Similar to our description, the natural 20% Mn-bearing norsethite reported by Zidarov et al. (2009) was transparent, colorless or pale-yellow, and had a vitreous luster.

Chemical composition is important for crystal structure refinement by single crystal XRD. A thin section was prepared from the $BaMn(CO_3)_2$ single crystals and used to quantify micro-composition using an electron probe analysis. Figure 3 illustrates the backscattering electron (BSE) and the detection position on the thin section. The results of the Ba and Mn content analysis are provided in Table 1. When compared with the BSE images using MnO_2 and $BaSO_4$ as the standard samples, it was observed that the gray scales of the polished single crystal surfaces were nearly identical, implying that the single crystals were uniform in composition. A total of 15 points at five different areas (marked by red circles) were selected for the electron probe analysis. The average wt% of BaO was 49.06(±0.04)% and 22.71(±0.02)% for MnO with standard deviations of less than 0.1%. Thus, the composition of the crystals is in excellent agreement with the ideal formula $Ba_{1.0}Mn_{1.0}(CO_3)_2$.

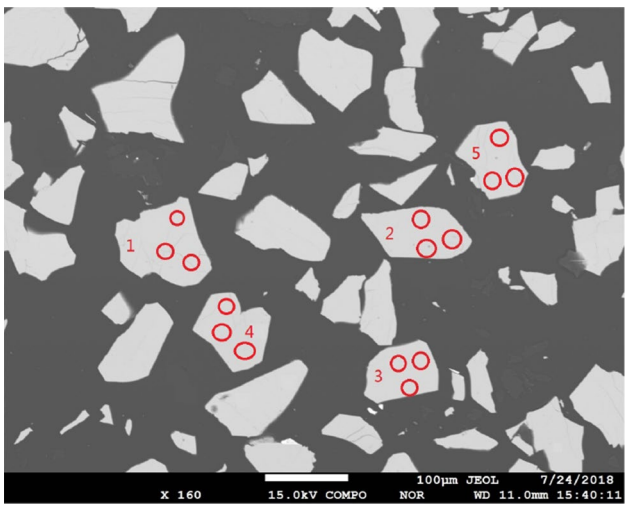

Fig. 3 The backscattered electronic (BSE) image of $BaMn(CO_3)_2$ single crystals thin section, in which the red circles are the detection position of electron probing

Single crystal XRD and crystal structure analysis of norsethite-type $BaMn(CO_3)_2$

The crystal structure of norsethite-type $BaMn(CO_3)_2$ was determined using single crystal XRD. The crystal data and structural refinement, including lattice parameters, positional and thermal properties, and bond length and angle, are summarized in Table 2; results are given for the average structure as no superlattice reflections were observed (space-group $R\bar{3}m$). In addition, Table 2 includes the structure refinement of $BaMg(CO_3)_2$ based on space-group symmetry $R\bar{3}c$ ($c' = 2c$) for comparison of the anisotropic displacement

Table 1 Composition of $BaMn(CO_3)_2$ single crystal

BaO and MnO (wt%)	Position 1		Position 2		Position 3		Average wt%		Standard wt%		Deviations	
Region 1	49.08	22.71	49.08	22.72	49.09	22.73	49.08	22.72	49.09	22.72	−0.01	0.00
Region 2	49.07	22.69	49.09	22.71	49.07	22.72	49.08	22.71	49.09	22.72	−0.01	−0.01
Region 3	49.09	22.70	49.08	22.73	49.08	22.73	49.09	22.72	49.09	22.72	0.00	0.00
Region 4	49.05	22.70	49.03	22.68	49.02	22.68	49.03	22.69	49.09	22.72	−0.06	0.03
Region 5	49.02	22.71	49.05	22.66	49.00	22.74	49.02	22.70	49.09	22.72	−0.07	−0.02
Average	–	–	–	–	–	–	49.06	22.71	49.09	22.72	−0.03	−0.01

Table 2 $BaMn(CO_3)_2$ single crystal structure

Lattice parameters

	Space group	*a*	*c*	*α*	*β*	*γ*	*V*	*R*	Ref.
$BaMn(CO_3)_2$	$R\bar{3}m$	5.0827(2)	17.2797(10)	90	90	120	386.59(4)	0.0184	This work
$BaMn(CO_3)_2$	$R\bar{3}c$	5.0834(4)	34.554(3)	90	90	120	773.29(11)	0.0444	This work
$BaMg(CO_3)_2$	$R\bar{3}c$	5.0212(9)	33.581(6)	90	90	120	733.2	0.0144	Effenberger et al. (2014)

Positional and thermal parameters

$BaMn(CO_3)_2$ ($R\bar{3}m$)

Parameters	Ba	Mn	C	O
x	0	0	0	0.1430(4)
y	0	0	0	−0.1430(4)
z	0	1/2	0.2410(4)	0.2445(2)
U11	0.0106(2)	0.0091(5)	0.013(2)	0.080(3)
U22	0.0106(2)	0.0091(5)	0.013(2)	0.080(3)
U33	0.0142(3)	0.0122(7)	0.011(3)	0.0264(17)
U23	0.0000	0.0000	0.0000	−0.0027(7)
U13	0.0000	0.0000	0.0000	0.0027(7)
U12	0.00532(12)	0.0046(2)	0.0067(11)	0.075(3)

Bond length (Å) and bond angle (°)

	$BaMn(CO_3)_2$ ($R\bar{3}m$)	$BaMn(CO_3)_2$ ($R\bar{3}c$)	$BaMg(CO_3)_2$ (Effenberger et al. 2014)
(Ba–O)1	2.9763(18)	2.919(13)	2.819(5)
(Ba–O)2	2.9764(18)	3.051(17)	3.087(5)
Mn(Mg)–O	2.149(4)	2.141(8)	2.0633(15)
C–O	1.260(4)	1.261(8)	1.2797(16)
O–Ba–O (*β*1)	62.73(11)	63.3(2)	66.86(13)
O–Ba–O (*β*2)	95.79(8)	94.4(4)	92.92(9)
O–Ba–O (*β*3)	121.64(15)	121.7(3)	123.59(7)
O–Ba–O (*β*4)	137.03(15)	137.2(3)	137.56(8)
O–Mn(Mg)–O (*α*1)	84.97(15)	85.5(4)	86.82(6)
O–Mn(Mg)–O (*α*2)	95.03(15)	91.7(8)	93.18(6)
O–Mn(Mg)–O (*α*3)	180.00(14)	175.9(9)	180.0
O–C–O	119.77(6)	119.91(16)	119.92(1)

parameters. The cif-files for the two structure models are attached as supplementary material.

Effenberger et al. (2014) found weak superstructure reflections along the c^* direction for $BaMg(CO_3)_2$ as observed in the reciprocal space reconstructed from X-ray images. Consequently, a doubling of the lattice parameter c was necessary. However, no such superstructure reflections were observed in the X-ray images of $BaMn(CO_3)_2$ even with a highly sensitive X-ray detector (supplementary Fig. 2). Therefore, a structure model with a doubled lattice parameter c was not applied for the refinement of the crystalline structure of $BaMn(CO_3)_2$. Even so, to better understand the structure, a doubled c model was used to refine the crystalline structure of $BaMn(CO_3)_2$. The lattice parameters and cell volume of $BaMn(CO_3)_2$ as well as the geometry of the (BaO_{12}) polyhedron were somewhat different from that of $BaMg(CO_3)_2$ owing to the substitutional variations of Mg^{2+} by Mn^{2+} cations. The O–C–O bond angle identified as 119.91(16)° for $BaMn(CO_3)_2$ and 119.92(1)° for $BaMg(CO_3)_2$ showed almost no difference, and the C-O bond distance of 1.261(8) Å in $BaMn(CO_3)_2$ was relatively shorter than the 1.2797(16) Å bond in $BaMg(CO_3)_2$.

However, some unreasonable issues remain for these refinement results. In the absence of any superstructure reflections from the X-ray images of the $BaMn(CO_3)_2$, both c and doubled c could well-describe the periodicity along the [001] direction. In accordance with the rules of crystallography, having a smaller periodicity, $\boldsymbol{c}$ should be applied to the structural unit. Most importantly, because O–Mn–O ($\alpha 3$) of 175.9(9)° does not equal 180°, it indicates that the Mn atom is located in the center of the MnO_6 octahedron as the Mn atom is located at position 6(b) with site symmetry $\bar{3}$. The difference between the structure refinement in space-group $R\bar{3}m$ (cell parameter c) and $R\bar{3}c$ (cell parameter $c'=2c$) is a result of the different multiplicities and site symmetries for the Ba and Mg atoms: $R\bar{3}m$ [Ba atoms at 3(a), site symmetry -32/m, Mn atoms at 3(b), site symmetry -32/m]; and $R\bar{3}c$ [Ba atoms at 6(a), site symmetry 32, Mn atoms at 6(b), site symmetry -3]. The release of symmetry elements enables different results. Hence, the refinement using the doubled c model is believed to be unnecessary for the $BaMn(CO_3)_2$ crystal structure when the additional superlattice is not observed.

On this basis, $R\bar{3}m$ is the most probable choice for the $BaMn(CO_3)_2$ crystal structure, and is consistent with previous results for norsethites (Effenberger and Zemann 1985; Secco and Lavina 1999). Figure 4 shows the rhombohedral crystal structure of $R\bar{3}m$ for $BaMn(CO_3)_2$ as well as the coordination relations. The unit cell consists of the (MnO_6) octahedron, (BaO_{12}) polyhedron, and CO_3^{2-} anions. These (MnO_6) octahedrons and (BaO_{12}) polyhedrons display periodically alternating layers stacked precisely above each other, parallel to the [001] direction, and separated by the

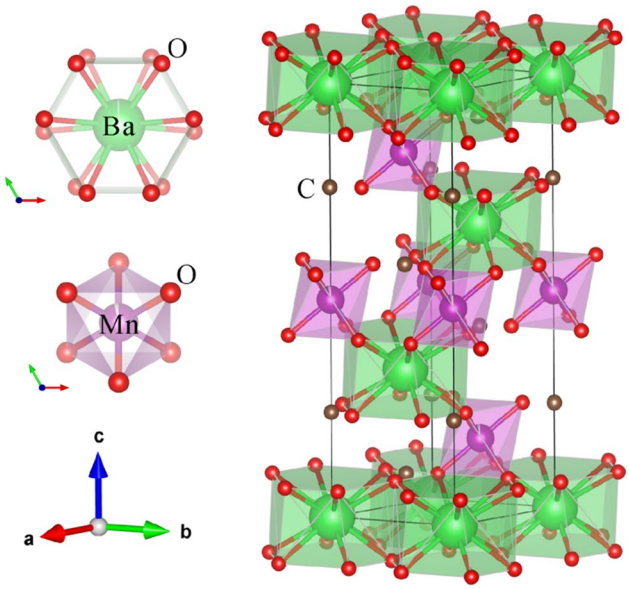

Fig. 4 The crystal structure of $BaMn(CO_3)_2$ as well as the coordination relations

triangular CO_3^{2-} groups. Table 2 gives the detailed structural parameters for $BaMn(CO_3)_2$. Obviously, the R value of 0.0184 using $R\bar{3}m$ is much smaller than the 0.0444 obtained for $R\bar{3}c$. The (Ba–O)1 and (Ba–O)2 bond distances show almost no difference, indicating the coordination number of the Ba^{2+} cation is 12, and not 6 + 6 as obtained from the doubled c model. The O–C–O bond angle is identified as 119.77(6)° for $BaMn(CO_3)_2$, which deviates from the standard bond angle of 120° observed in simple calcite-type carbonates.

To date, the controversy over the structure of norsethite $BaMg(CO_3)_2$ and norsethite-type $BaMn(CO_3)_2$ is focused on whether or not the additional superlattice exists. This problem is related to the displacement of the O atoms in the lattice, thereby determining the space-group as $R\bar{3}c$ or $R\bar{3}m$ for the structure refinement. Based on the results from the X-ray images, the superlattice was not observed in the $BaMn(CO_3)_2$ structure. However, this does not preclude the existence of $BaMn(CO_3)_2$ single crystals with a superlattice because the crystal quality is strongly dependent on the growth environment. As well as quenching the operation, a high P–T reaction could be propitious to the formation of some metastable phases. Exactly, there are two polymorphs that can be maintained in norsethite-type structure resulting from different growth environments: (1) $R\bar{3}c$ stable phase with oxygen ordering is obtained for $BaMg(CO_3)_2$ synthesized at ambient conditions (Lippmann 1968; Effenberger et al. 2014); (2) $R\bar{3}m$ metastable phase with oxygen disordering is adopted for $BaMn(CO_3)_2$ synthesized at high P–T conditions while quenched to ambient conditions. The disordering phase might be caused by a rapid quenching of the

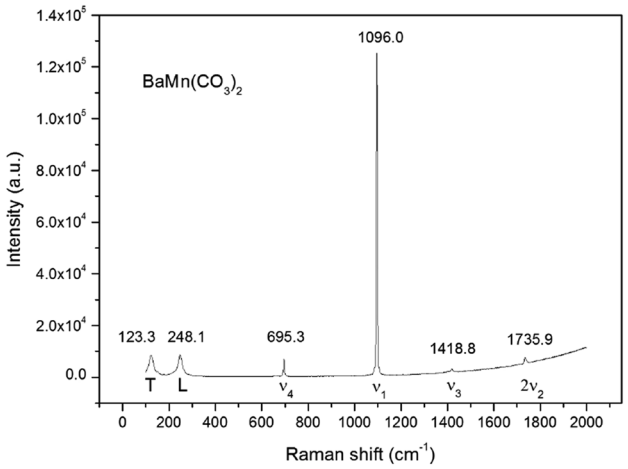

Fig. 5 Raman spectra of $BaMn(CO_3)_2$ single crystal at ambient conditions

samples during high P–T reaction. In this regard, of particular interest is the possibility of obtaining oxygen ordering phase after annealing the oxygen disordering phase at high temperature and ambient pressure for several weeks, which deserves further probing.

Up till now, there has not been any structure refinement of natural norsethite that would allow the observation of superstructure reflections (Secco and Lavina 1999; Zidarov et al. 2009). Superstructure reflections are caused by the order of the rotation of the carbonate groups only. Due to the small scattering power of the O atoms compared to that of the Ba atoms, the intensity of the superstructure is quite small; therefore, a highly sensitive detector is required. Conventional X-ray detectors do not allow the registration of such minor intensities by powder or single crystal diffraction.

Pressure-induced transition of $BaMn(CO_3)_2$ investigated by Raman spectroscopy

The developed $BaMn(CO_3)_2$ single crystals were large enough for micro-Raman spectroscopy, and a piece of crystal with a flat surface was selected for the measurements at ambient conditions. Six vibrational modes were observed in the wavenumber range from 100 to 2000 cm^{-1}, which is similar to other rhombohedral carbonates (White 1974; Bischoff et al.1985). The Raman peaks were fit with a Lorentzian function located at 123.3, 248.1, 695.3, 1096.0, 1418.8, and 1735.9 cm^{-1}, as shown in Fig. 5. Two lattice modes at 123.3 cm^{-1} and 248.1 cm^{-1} were derived mainly from the translational lattice mode T and vibrational lattice mode

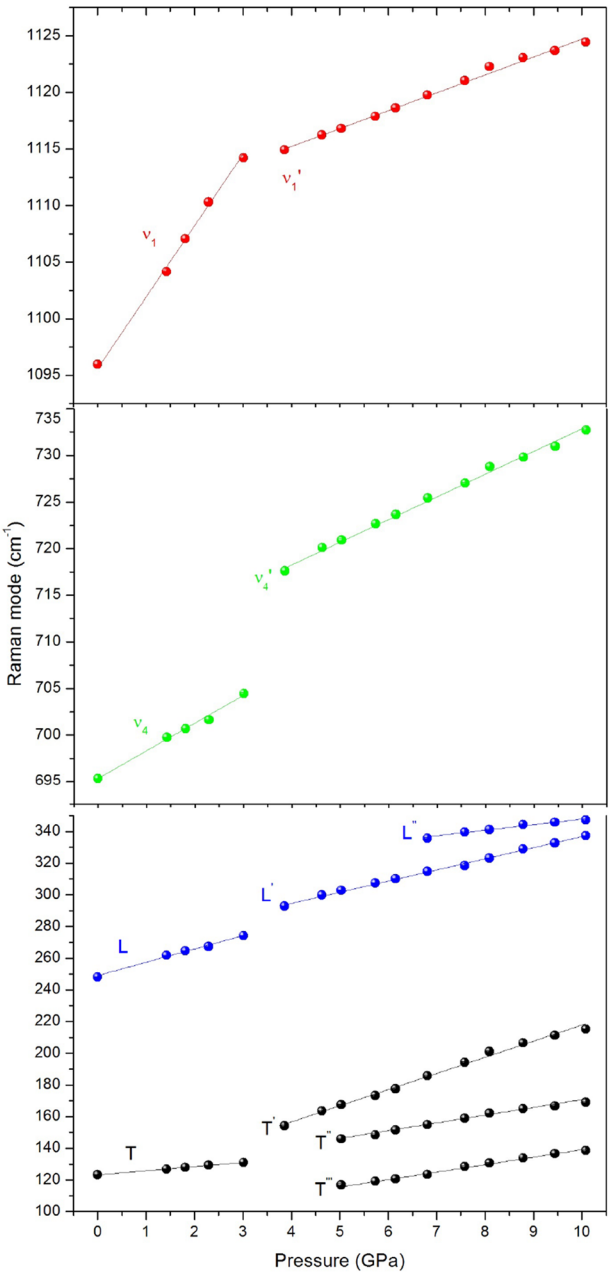

Fig. 6 High-pressure Raman spectra of $BaMn(CO_3)_2$ at room temperature

Table 3 Raman spectra of $BaMn(CO_3)_2$ single crystal

T (cm^{-1})	L (cm^{-1})	ν_4 (cm^{-1})	ν_1 (cm^{-1})	ν_3 (cm^{-1})		$2\nu_2$ (cm^{-1})		Refrences
123.26(10)	248.15(12)	695.33(3)	1095.97(3)	1418.76(11)		1735.89(27)		This work
124.2 (1.0)	248.5 (3.4)	696.5 (0.8)	1097.1 (0.8)	1399.0 (4.4)	1419.5 (1.3)	1734.3 (2.0)	1737.6 (2.0)	Schmidt et al. (2013)

L, respectively. The peaks at 695.3, 1096.0, 1418.8, and 1735.9 cm^{-1} were attributed to the in-plane bending internal mode ν_4, the symmetric stretching internal mode ν_1, the anti-symmetric stretching mode ν_3, and out-of-plane bending mode $2\nu_2$, respectively. Compared with the previous results reported by Schmidt et al. (2013), there are slight differences in all the Raman peak positions, as given in Table 3. This could be caused by the systematic errors of the measuring device. Moreover, Schmidt et al. (2013) observed an obvious splitting of the ν_3 and $2\nu_2$ modes, which, we speculate, may be induced by the residual stress in the high P–T synthetic sample. In contrast, no splitting was found in our experiments because the water fluid greatly reduced the residual stress in the single crystals.

The high-pressure Raman spectra of the $BaMn(CO_3)_2$ single crystal was measured in the diamond window of 100–1200 cm^{-1} at ambient temperatures, and the hydrostatic pressure was increased up to 10–0.5 GPa increments. The Raman shifts that occurred as a function of pressure $\nu_i(P)$ are shown in Fig. 6 while the corresponding mode positions and slopes $d\nu_i/dP$ are presented in Tables 4 and 5. The $BaMn(CO_3)_2$ before and after the pressure-induced transition are assigned to $BaMn(CO_3)_2$ I and $BaMn(CO_3)_2$ II. Pressures at and below 3.0 GPa had T, L, ν_4, and ν_1 modes increasing linearly with the increasing pressure and did not undergo any resolvable splitting. When the pressure reached up to 3.8 GPa, the T and L modes experienced splitting of different degrees while the values of the slope $d\nu_i/dP$ for each Raman vibration changed drastically. The T mode split into three new modes T', T'' and T''' and the corresponding $d\nu_i/dP$ changed from 2.60(5) to 10.19(5) cm^{-1}/GPa, 4.90(6) cm^{-1}/GPa, and 4.90(10) cm^{-1}/GPa. Similarly, the L mode split into two new modes L' and L'', and the correlated $d\nu_i/dP$ was fit as 7.02(2) cm^{-1}/GPa and 3.49(21) cm^{-1}/GPa, differing from the original value of 8.40(5) cm^{-1}/GPa. Meanwhile, the ν_4 and ν_1 modes exhibited an obvious jump and the $d\nu_i/dP$ changed significantly.

According to these results, there is strong evidence that the norsethite-type $BaMn(CO_3)_2$ underwent a certain pressure-induced transition at a critical transition pressure between 3.0 and 3.8 GPa. Similarly, Pippinger et al. (2014) reported that a pressure-induced transition occurred at approximately 2.32 GPa in $BaMg(CO_3)_2$ and the novel

Table 4 High-pressure Raman spectra of $BaMn(CO_3)_2$ single crystal

P, σ_P (GPa)	T (cm^{-1})	L (cm^{-1})	ν_4 (cm^{-1})	ν_1 (cm^{-1})
1 atm	123.26(10)	248.15(12)	695.33(3)	1095.97(3)
1.42(0)	126.90(13)	261.82(8)	699.76(5)	1104.16(2)
1.81(0)	127.98(18)	264.57(7)	700.67(6)	1107.06(2)
2.29(3)	129.27(13)	267.34(9)	701.64(10)	1110.30(2)
3.01(2)	131.06(17)	274.27(12)	704.47(11)	1114.22(2)

Phase transition	T' (cm^{-1})	T'' (cm^{-1})	T''' (cm^{-1})	L' (cm^{-1})	L'' (cm^{-1})	ν_4' (cm^{-1})	ν_1' (cm^{-1})
3.86(3)	154.16(32)	–	–	292.89(9)	–	717.60(4)	1114.92(2)
4.63(3)	163.51(34)	–	–	299.91(16)	–	720.12(6)	1116.24(2)
5.03(6)	167.47(32)	116.83(95)	145.88(36)	302.93(13)	–	720.92(8)	1116.8(4)
5.73(3)	173.28(36)	119.15(42)	148.47(37)	307.45(13)	–	722.67(6)	1117.87(2)
6.15(2)	177.47(50)	120.66(41)	151.56(36)	310.24(13)	–	723.67(6)	1118.61(3)
6.81(4)	185.71(37)	123.49(32)	154.95(35)	314.74(23)	335.73(61)	725.44(9)	1119.76(3)
7.58(2)	194.26(39)	128.48(55)	158.94(18)	318.45(13)	339.66(41)	727.03(10)	1121.03(3)
8.09(3)	201.05(32)	130.67(31)	162.12(21)	323.21(17)	341.20(31)	728.78(6)	1122.28(3)
8.78(2)	206.46(30)	133.89(61)	164.99(17)	328.97(18)	344.41(53)	729.80(8)	1123.06(3)
9.44(4)	211.23(34)	136.57(30)	166.73(32)	332.76(16)	345.83(61)	730.97(7)	1123.68(2)
10.08(3)	215.25(39)	138.51(53)	169.09(28)	337.31(15)	347.22(63)	732.72(8)	1124.43(3)

Table 5 $\frac{d\nu_i}{dP}$ of $BaMn(CO_3)_2$ single crystal

$BaMn(CO_3)_2$	I	I	I	I	II	II	II	II	II	II	II
Raman modes	T	L	ν_4	ν_1	T'	T''	T'''	L'	L''	ν_4'	ν_1'
$\frac{d\nu_i}{dP}$ (cm^{-1}/GPa)	2.60(5)	8.40(5)	2.97(2)	6.30(2)	10.19(5)	4.90(6)	4.90(10)	7.02(2)	3.49(21)	2.46(1)	1.58(1)

$BaMg(CO_3)_2$ II was identified as the *C*2/*c* structure. Due to the similarity in the crystal structures, we infer that the $BaMn(CO_3)_2$ II may have similar structures to the $BaMg(CO_3)_2$ II, but still requires future determination from single crystal synchrotron XRD.

Conclusion

Since no superlattices were observed in the X-ray images, the structure of norsethite-type $BaMn(CO_3)_2$ obtained under high P–T conditions was confirmed as the $R\bar{3}m$ space-group from the single crystal XRD measurements, and not the $R\bar{3}c$ space-group with a doubled *c*-axis. However, because it is believed to be dependent on the formation environment, the existence of the superlattice is still an ongoing debate for norsethite and norsethite-type structures. Thus, it is proposed that the single crystals of $BaMg(CO_3)_2$ be prepared under high P–T conditions to confirm the metastable phase with oxygen disordering, which is absolutely necessary for better comparisons with the stable phase with oxygen ordering reported by Effenberger et al. (2014). As a further extension, the structure and properties of the solid solution Ba(Mg, Mn)$(CO_3)_2$ with various Mn content will be investigated and quantified in the future, and the results could enhance the current understanding of natural norsethite carbonates.

Acknowledgements We appreciate Herta Effenberger and other two anonymous reviewers for their valuable comments and suggestions, which are important to greatly improve the manuscript quality. We also acknowledge Jung-Fu Lin from University of Texas at Austin for constructive discussion in carbonates minerals. This work was financially supported by Major State Research Development Program of China (2016YFC0601101), the National Science Foundation for Young Scientists of China (41802044), the Strategic Priority Research Program (B) of Chinese Academy of Sciences (XDB 18010401), 135 Program of the Institute of Geochemistry (Y2ZZ041000), CAS, and the Western Light (Y8CR028).

References

Bischoff WD, Sharma SK, MacKenzie FT (1985) Carbonate ion disorder in synthetic and biogenic magnesian calcites: a Raman spectral study. Am Miner 70:581–589

Böttcher ME (2000) Stable isotope fractionation during experimental formation of norsethite ($BaMg[CO_3]_2$): a mineral analogue of dolomite. Aquat Geochem 6:201–213

Böttcher ME, Effenberger HS, Gehlken P-L, Grathoff GH, Schmidt BC, Geprägs P, Bahlo R, Dellwig O, Leipe T, Winde V, Deutschmann A, Stark A, Gallego-Torres D, Martinez-Ruiz F (2012) $BaMn[CO_3]_2$—a previously unrecognized double carbonate in low-temperature environments: structural, spectroscopic, and textural tools for future identification. Chem Erde 72:85–89

Chang LLY (1964) Synthesis of $MBa(CO_3)_2$ compounds. Am Miner 49:1142–1143

Damyanov ZK, Bakardjiev S, Popov P (1996) Mineralogy, geology and genesis of the Kremikovtsi carbonate-hosted submarine exhalative iron(+Mn)–barite (+base metals) deposit, West Balkan, Bulgaria. In: Proceedings of the Ann. Meet., Sofia, 1996, UNESCO Project 356, vol 1, pp 29–37

Effenberger H, Zemann J (1985) Single crystal X-ray investigation of norsethite, $BaMg(CO_3)_2$: one more mineral with an aplanar carbonate group. Zeitschrift fu¨r Kristallographie 171:275–280

Effenberger H, Pippinger T, Libowitzky E, Lengauer CL, Miletich R (2014) Synthetic norsethite, BaMg(CO3)2: revised crystal structure, thermal behaviour and displacive phase transition. Mineral Mag 78(7):1589–1612

Hood WC, Steidl PF, Tschopp DG (1974) Precipitation of norsethite at room temperature. Am Miner 59:471–474

Kapustin JL (1965) Norsethite—the first find in USSR. Doklady Acad Nauk USSR 161:922–924 **(in Russian)**

Lepland A, Stevens RL (1998) Manganese authigenesis in the landsort deep, Baltic Sea. Mar Geol 151:1–25

Lepland A, Sætherc O, Thorsnes T (2000) Accumulation of barium in recent Skagerrak sediments: sources and distribution controls. Mar Geol 163:13–26

Liang W, Yin Y, Li Z, Li R, Li L, He Y, Dong H, Li Z, Yan S, Zhai S, Li H (2018) Single crystal growth, crystalline structure investigation and high-pressure behavior of impurity-free siderite ($FeCO_3$). Phys Chem Miner 45(9):831–842

Lindner M, Jordan G (2018) On the growth of witherite and its replacement by the Mg-bearing double carbonate norsethite: implications for the dolomite problem. Am Miner 103:252–259

Lindner M, Saldi GD, Jordan G, Schott J (2017) On the effect of aqueous barium on magnesite growth—a new route for the precipitation of the ordered anhydrous Mg-bearing double carbonate norsethite. Chem Geol 460:93–105

Lindner M, Saldi GD, Carrocci S, Be´ne´zeth P, Schott J, Jordan G (2018) On the growth of anhydrous Mg-bearing carbonates—implications from norsethite growth kinetics. Geochim Cosmochim Acta 238:424–437

Lippmann F (1968) Die Kristallstruktur von Norsethit. Tschermaks Mineral Petrogr Mitt 12:299–318

Mrose ME, Chao ETC, Fahey JJ, Milton C (1961) Norsethite, $BaMg(CO_3)_2$, a new mineral from the Green River formation, Wyoming. Am Miner 46:420–429

Onac BP (2002) Caves formed within Upper Cretaceous skarns at Băiţa, Bihor County, Romania: mineral deposition and speleogenesis. Can Mineral 40:1693–1703

Peacor DR, Essene EJ, Gaines AM (1987) Petrologic and crystal-chemical implications of cation order-disorder in kutnahorite $CaMn(CO_3)_2$. Am Miner 72:319–328

Pippinger T, Miletich R, Effenberger H, Hofer G, Lotti P, Merlini M (2014) High-pressure polymorphism and structural transitions of norsethite, $BaMg(CO_3)_2$. Phys Chem Miner 41:737–755

Platt RG, Woolley AR (1990) The carbonatites and fenites of Chipman lake, Ontario. Can Mineral 28:241–250

Reeder RJ (1983) Crystal chemistry of the rhombohedral carbonates. In: Reeder RJ (ed) Carbonates: mineralogy and chemistry. Reviews in mineralogy, vol 11. Mineralogical Society of America, Washington, pp 1–48

Reeder RJ, Dollase WA (1989) Structural variation in the dolomite-ankerite solid-solution series: an X-ray, Moessbauer, and TEM study. Am Miner 74:1159–1167

Ross NL, Reeder RJ (1992) High-pressure structural study of dolomite and ankerite. Am Miner 77:412–421

Schmidt B, Gehlken PL, Böttcher ME (2013) Vibrational spectra of $BaMn(CO_3)_2$ and a re-analysis of the Raman spectrum of $BaMg(CO_3)_2$. Eur J Mineral 25:137–144

Secco L, Lavina B (1999) Crystal chemistry of two natural magmatic norsethites, BaMg(CO3)2, from an Mg-carbonatite of the alkaline carbonatitic complex of Tapira (SE Brazil). Neues Jahrb Mineral Monatsh 1999:87–96

Sheldrick GM (2008) A short history of SHELX. Acta Cryst. A 2008(64):112–122

Steyn JGD, Watson MD (1967) A new occurrence of norsethite, $BaMg(CO_3)_2$. Am Miner 52:1770–1775

Sundius N, Blix R (1965) Norsethite from Langban. Arkiv Mineral Geol 4:277–278

White WB (1974) The carbonate minerals. In: Farmer VC (ed) The infra-red spectra of minerals, Mineralogical Society monograph, vol 4. Mineralogical Society, London, pp 227–284

Zheng YF, Böttcher ME (2014) Oxygen isotope fractionation in double carbonates. Isot Environ Health Stud 52:29–46

Zidarov N, Petrov O, Tarassov M, Damyanov Z, Tarassova E, Petkova V, Kalvachev Y, Zlatev Z (2009) Mn-rich norsethite from the Kremikovtsi ore deposit, Bulgaria. N Jb Mineral Abh 186:321–331